Fuel 107 (2013) 525–538

Contents lists available at SciVerse ScienceDirect

Fuel

journal homepage: www.elsevier.com/locate/fuel

Frontal stability of reactive nanoparticle transport during *in situ* catalytic upgrading of heavy oil

Karim Ghesmat, Hassan Hassanzadeh *, Jalal Abedi, Zhangxin Chen

Department of Chemical and Petroleum Engineering, Schulich School of Engineering, University of Calgary, Calgary, AB, Canada T2N 1N4

HIGHLIGHTS

- Increasing the reaction rate promotes instability around an interface delivering nano-catalysts.
- Increasing the nano-catalysts deposition rate stabilizes the displacement front.
- Accumulation of nano-catalysts behind the front can destabilize the reactive front.

ARTICLE INFO

Article history:
Received 22 August 2012
Received in revised form 16 November 2012
Accepted 19 November 2012
Available online 8 December 2012

Keywords:
Nanoparticles
Instability
Porous media
Heavy oil upgrading
Miscible flow

ABSTRACT

The application of nanoparticles as a catalyst in porous media has recently been increased and is generally relevant to applications that include *in situ* heavy oil upgrading and removal of reactive and non-reactive pollutants in groundwater. The objective of this paper is investigation of the effects of reactive nano-catalysts on viscous fingering instability. In order to understand the behaviour of frontal instabilities during transport of reactive nanoparticles, the basic equations of conservation of mass and momentum are linearized and solved numerically. The analysis reveals that increasing the reaction rate promotes the viscous fingering instability around an interface delivering nano-catalysts, while increasing the nano-catalysts deposition rate usually stabilizes the displacement front. It is also shown that accumulation of nano-catalysts behind the front can destabilize the reactive front. The effects of the interface sharpness, nanoparticles diffusion coefficient, permeability of porous media, and viscosity ratios of different phases are also discussed.

1. Introduction

The transport of nanoparticles in porous media has recently garnered attention in many studies [1–4]. Despite their minuscule state, nanoparticles may hold the potential to cost-effectively address some of the challenges of *in situ* heavy oil and bitumen upgrading and also site remediation. Two factors contribute to nanoparticles' capabilities as an extremely versatile tool. The first is their small particle sizes (1–100 nm). Nanoparticles can be effectively transported in porous media by the flow either by injection or by gravity. Nanoparticles can also remain as a suspension for extended periods of time to establish an *in situ* treatment zone.

Equally important, they provide enormous flexibility for both *in situ* and *ex situ* applications. For example, nanoparticles are easily deployed in slurry bioreactors for treatment of contaminated soils, sediments and solid wastes. The technology holds great promise for mobilizing heavy oil and bitumen, which is currently a big challenge in the oil industry.

Major characteristics of nanoparticles that determine the applicability of nano-materials in porous media are their mobility and reactivity. In fact, the higher mobility and reactivity of the nanoparticles provide greater potential for exposure, as nanomaterials disperse over greater distances and promote their effective persistence in the environment.

The problem of reaction in porous media using nano-catalysts has recently been the subject of many studies in three main categories, including transport optimization [1,5,6], particle deposition and aggregation [7–10], and testing of different nano-materials as catalysts [11]. Although extensive experimental works have been conducted, there are still only a few analytical and numerical studies of such systems [12].

One of the major challenges in modeling these systems is finding appropriate correlations to predict deposition kinetics of nanoparticles in porous media and also the change of permeability and porosity. One phenomenon that may reduce nanoparticles' exposure is a tendency to attach to the surface (deposition), as well as to each other (aggregation). The deposition kinetics of nano and micro scale particles has already been reviewed by many authors. A number of predictive models were developed essentially by following the filtration equations proposed by Iwasaki [13], and a

* Corresponding author. Tel.: +1 (403) 210 6645; fax: +1 (403) 282 4852.
E-mail address: hhassanz@ucalgary.ca (H. Hassanzadeh).

0016-2361/$ - see front matter © 2012 Elsevier Ltd. All rights reserved.
http://dx.doi.org/10.1016/j.fuel.2012.11.061

significant advancement in the theoretical understanding of the process was achieved by Payatakes et al. [14] and Rajagopalan and Kim [15], who imparted a new theoretical insight to the empirical correlations developed in the past.

As a pioneering work, Spielman and Friedlander [16] presented a theoretical analysis to describe the deposition of Brownian particles that interact with collectors through an attractive–repulsive potential. They showed that, when the interactions are confined sufficiently near the collector surface, the process is equivalent to ordinary convection and diffusion in the bulk with a first-order surface reaction at the collector. Gruesbeck and Collins [17] also presented a simple model to predict entrainment and deposition of naturally occurring fine particles in porous media. The central concept of the theory was representation of both particle and pore size distributions by partitioning the porous medium at any cross section into parallel plugging and non-plugging pathways. Their simple model was shown to be adequate, as the validity was tested with experimental data.

Sharma and Yortsos [18] formulated a mathematical model for the transport of stable particulate suspensions in porous media, where a first-order kinetics model was presented for both release and deposition mechanisms of fine particles in the porous medium. Several other theoretical models for transport of the flow of particles with Brownian motion have been established and validated experimentally by many authors [19–21].

All of the mentioned parameters, such as deposition, aggregation, particle diffusion coefficient, and viscosity difference between phase and nanoparticle concentration, can have significant impact on the stability of the front when nanoparticles are used as nano-catalysts. Many studies have addressed the reactive and non-reactive front instability due to adverse viscosity in porous media both numerically and experimentally. As several authors have reported [22–25] when chemical reactions come into play, different fingering instability mechanisms can be expected. However, a clear understanding of how the addition of a nano-catalyst to the flow system and the physical properties of the nanoparticles can affect the stability has not yet been studied.

Among the first experimental studies that attempted to understand this fingering instability is the pioneering work of Hill [26]. Later studies by Saffman and Taylor [27] involved experimental analyses and physical explanations of the growth of the finger instability. Numerous subsequent studies analyzed the effects of surface tension [28], non-Newtonian rheological behavior of the fluids [29], transverse gravity fields [30], adsorption on a porous matrix [31], and a cell gap [32].

There has been equally rich activity dealing with the numerical and mathematical modeling of this fingering instability. Efforts in this field date back to at least the work of Peaceman and Rachford [33], who numerically modeled the nonlinear development of the flow for a rectilinear miscible displacement. Subsequent studies allowed for examination of the role of many factors, such as dispersion [34,35], viscosity ratio [36], density and viscosity distribution [37], gravity [38], effect of Brownian motion of sedimenting suspension [39], carbon dioxide (CO_2) sequestration [40–43], and reactive–dispersive behavior [35,44,45].

One of the difficulties that may be found in the use of nano-catalysts in porous media is the front stability. The stability of the front at the injection line can play an important role for the efficiency of the *in situ* process. In some processes, such as the convective mixing of CO_2 in deep saline aquifers [43], the unstable front is usually favorable; whereas, it is unfavorable in most environmental and oil recovery relevant applications. There is still a lack of understanding on how the addition of nanoparticles into the carrier phase may affect the front stability.

In a recent study we have studied the effect of nonreactive nanoparticles on dynamics of miscible flows [12]. In this work, we extend our previous study to reactive nanoparticles and address how the viscous fingering instability of a front may be affected by the addition of nano-catalysts into the flow system right behind the injection line. The effects of the nanoparticle diffusion coefficient, deposition rate, reaction rate, viscosity ratios of displaced and displacing fluids, and permeability change are discussed. Readers should note that the current work is different from classic viscous fingering works [22,23,34–36], where an interface is considered in the middle of low and high viscous fluids, the domain of which is extended to infinity from both side, $x \in [-\infty, \infty]$. In contrast to previous viscous fingering studies, in the current study, the interface is at the injection line and the domain is finite, $x \in [0, Pe]$. This makes the problem different from both physics and mathematical points of view.

The other difference between this work and others on reactive flow in porous media is that this paper is an attempt to understand the role of nano-catalysts on the fingering instability of miscible flows. Particles are considered to play the role of catalysts and to expedite the chemical reaction.

2. Mathematical model

We consider a horizontal displacement involving a Newtonian incompressible fluid in a homogeneous porous medium. A schematic of the flow geometry is shown in Fig. 1. The porous medium is initially saturated with pseudo-component b, which is assumed to undergo a cracking reaction. The nano-catalyst solution is injected at the injection line, shown by the value of zero on the x-axis in Fig. 1. This geometry and position of interface makes this problem different from classic works of viscous fingering [37].

The reaction can take place using nano-catalyst particles (components c) in the displacing or carrier fluid. The displacing fluid is a pseudo-component called component a. It is usually expected that several components are produced when the cracking reaction takes place as shown in:

$$b + c \rightarrow a_1 + a_2 + \cdots + a_n + c \tag{1}$$

In order to simplify the problem, we consider all the products $(a_1, \ldots a_n)$ as a pseudo-component, a. The pseudo component is considered as a fluid with averaged physical properties of all produced components. The product of the reaction is also component a and is assumed to have a high concentration behind the front and can be considered as the displacing fluid. One representative example can be the injection of a less viscous hydrocarbon as a displacing fluid delivering nanoparticle catalysts into a heavy oil reservoir. The heavy oil undergoes the cracking reaction and produces less viscous hydrocarbon. In this case, as given by Levenspiel [46] for homogeneous catalyzed reactions, the equation is simply:

$$b + c \rightarrow a + c \tag{2}$$

The nano-catalysts are usually injected into the reservoirs or subsurface in very low concentrations and are diluted solutions [7,12]. This is the reason that we may assume that the catalyst particles that are nano sized have Brownian motion in the medium. The carrier phase, including the nano-catalysts, with a viscosity of μ_0 initially displaces the original fluid with a viscosity of μ_1. The system is modeled using Darcy's law, the continuity equation, and equations of convection–diffusion–reaction for components a and b. Assuming a constant porosity, the equation of motion and governing equations for components a and b are shown as follows:

$$\mathbf{u} = -\frac{K}{\varphi\mu}\nabla p \tag{3}$$

$$\nabla \cdot \mathbf{u} = 0 \tag{4}$$

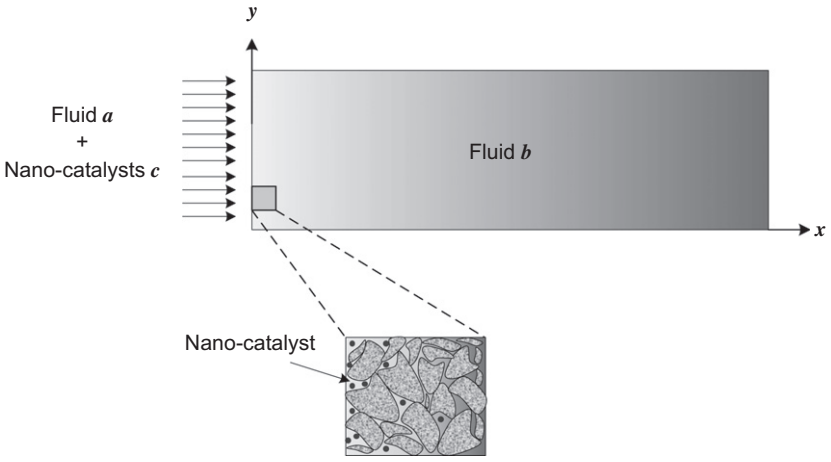

Fig. 1. Schematic of nano-reactive front displacement in porous media.

$$\frac{\partial c_a}{\partial t} + \mathbf{u}\cdot\nabla c_a = D_a\nabla^2 c_a + k_r c_c c_b \tag{5}$$

$$\frac{\partial c_b}{\partial t} + \mathbf{u}\cdot\nabla c_b = D_b\nabla^2 c_b - k_r c_c c_b \tag{6}$$

where $\mathbf{u}(u,v)$, p, c, μ and K represent the two-dimensional interstitial velocity vectors, pressure, component concentration, viscosity and medium permeability, respectively. In the above set of equations, D_a, D_b, and k_r represent the diffusion coefficients of components a and b and the reaction rate constant for the reaction, respectively.

The governing equation for the concentration distribution of Brownian particles over a surface in the presence of interaction forces is [47,16]:

$$\frac{\partial c_c}{\partial t} + \mathbf{u}\cdot\nabla c_c = \nabla\cdot(D_P\nabla c_c + mc_c\nabla\Phi) \tag{7}$$

where c_c, is the particle concentration, D_P is the nanoparticle diffusion coefficient, m is the particle mobility, and Φ represents the total colloidal interaction energy.

There are several relationships presented in the literature for the nano and micro scale interaction of the particles in a porous medium ($R_i = \nabla\cdot(mc_c\nabla\Phi)$). This interaction usually results in the deposition and release of particles to or from the medium [17,18,48]. Some researchers relate the particle deposition and release to a critical velocity and others to the concentration of the particles in the medium. We select the formulation presented by Sharma and Yortsos [18], Chu et al. [49] and Jin et al. [50], where deposition of the particle is assumed at a constant rate and controlled by a first-order kinetic mechanism:

$$R_i = -k_{dep}c_c \tag{8}$$

where k_{dep} is positive and represents the deposition rate constant. The deposition rate constant, k_{dep}, depends on the molecular interaction and electrostatic forces; and, any change of these forces is reflected in this constant. It is necessary to mention that there is no published result regarding deposition of nanoparticles in heavy oil.

In this study, we assume that the initial concentrations of components a and b are equal to $c_{a0} = c_{b0}$ and the initial injection velocity is U_0. Viscosity is assumed as a function of the concentrations of all components (a, b and c), such that $\mu(a_0,0,0) = \mu_A$ and $\mu(0,a_0,0) = \mu_B$. The addition of nanoparticle catalysts is also assumed to affect the viscosity. The relationship between viscosity and concentration can be shown with functions used previously [22,35,36]. The viscosity of the solution can be even affected by nanoparticle addition when the particle concentration is enough large:

$$\mu = \bar{\mu}e^{(\alpha_a c_a + \alpha_b c_b + \alpha_c c_c)/a_0} \tag{9}$$

where α_a, α_b and α_c are log mobility ratios defined at concentration a_0. $\bar{\mu}$ is constant and solvent viscosity, and $\alpha_a = \ln(\mu_A/\bar{\mu})$, $\alpha_b = \ln(\mu_B/\bar{\mu})$ and $\alpha_c = \ln(\mu_C/\bar{\mu})$ are logarithmic mobility ratios.

The permeability may also change when nano-catalysts are deposited in the porous medium. This functionality can be considered as a nano-catalyst concentration change, such that $K(c_c = a_0) = K_c$ and $K(c_c = 0) = K_1$. It has been shown [7,21] that the nanoparticles may aggregate, resulting in deposition in the porous medium. Indeed, the areas with a higher concentration of nanoparticles may be imposed by a higher rate of deposition, resulting in a permeability reduction. This may lead us to assuming an arbitrary formulation, in which the permeability change is higher wherever the concentration of nanoparticles is higher. Although there is no solid mathematical relationship between permeability and concentration of nanoparticles in the literature, we may assume an exponential relationship, as given by Civan [51,52]:

$$K = \overline{K}e^{\beta c_c/a_0} \tag{10}$$

where β is a mobility ratio at particle concentration of a_0. $\overline{K}$ is also a constant. It is necessary to mention that the change of porosity is assumed to be negligible due to particle deposition.

For the entire study, the system is also studied in a reference moving at the velocity of the injection line, U_0:

$$\widehat{\mathbf{u}} = \mathbf{u} - U_0\mathbf{i} \tag{11}$$

For convenience, the equations are made dimensionless using a diffusion scale. Thus, we scale all lengths by the diffusion length, D_a/U_0, time by the diffusive time, D_a/U_0^2, viscosity by μ_0, permeability by K_0, concentration by a_0, and velocity by U_0. The domain length in the flow direction is also shown by the Peclet number, U_{0L}/D_a, using the above scaling criteria. By dropping all hats, the equations are then converted into:

$$\mathbf{u} + \mathbf{i} = -\frac{K}{\varphi\mu}\nabla p \tag{12}$$

$$\nabla\cdot\mathbf{u} = 0 \tag{13}$$

$$\frac{\partial c_a}{\partial t} + \mathbf{u}\cdot\nabla c_a = \nabla^2 c_a + Da\cdot c_b c_c \tag{14}$$

$$\frac{\partial c_b}{\partial t} + \mathbf{u}\cdot\nabla c_b = D_b^*\nabla^2 c_b - Da\cdot c_b c_c \tag{15}$$

$$\frac{\partial c_c}{\partial t} + \mathbf{u}\cdot\nabla c_c = D_P^*\nabla^2 c_c - Da_{dep} c_c \tag{16}$$

where Da represents a dimensionless reaction rate constant known as the Damköhler number; and, D_b^* and D_P^* are the dimensionless displaced fluid and nanoparticles diffusion coefficients, which are the ratios of the displaced fluid and nanoparticles diffusion coefficients to the displacing fluid diffusion coefficient. Da_{dep} also stands for dimensionless rate of nanoparticles deposition. Damköhler, Da, is $Da = D_a\cdot k_r\cdot a_0/U_0^2$ representing the ratio of reaction rate to the convection. Da_{dep} is $D_a\cdot k_{dep}/U_0^2$ and the same as Da it is representing the rate of mass transportation by deposition to the convection. It is necessary to mention that diffusion coefficients of nanoparticle in both fluids a and b are assumed to be equal as both displacing and displaced fluids are hydrocarbon and have usually similar physical properties such as density and diffusion coefficient. It is also attempted to find nanoparticles which have the same physical properties. As our study is also a parametric one, we assume diffusion coefficient of one and then analyze how it affects the front instability when it deviates from one.

In order to conduct a linear stability analysis, small perturbations are introduced into the system at the base state:

$$c(x,y,t) = c_0(x,t) + c'(x,y,t) \tag{17}$$

$$p(x,y,t) = p_0(x,t) + p'(x,y,t) \tag{18}$$

$$u(x,y,t) = u_0 + u'(x,y,t) \tag{19}$$

$$v(x,y,t) = v_0 + v'(x,y,t) \tag{20}$$

$$\mu(x,y,t) = \mu_0(x,t) + \mu'(x,y,t) \tag{21}$$

$$K(x,y,t) = K_0(x,t) + K'(x,y,t) \tag{22}$$

where the primed terms represent small perturbations from the base state. In the moving reference frame u_0 and v_0 are equal to zero.

First, a solution is sought for the base state by substituting Eqs. (17)–(22) into Eqs. (12)–(16). The resulting equations are:

$$\frac{\partial c_{a0}}{\partial t} = \frac{\partial^2 c_{a0}}{\partial x^2} + Da\cdot c_{c0}c_{b0} \tag{23}$$

$$\frac{\partial c_{b0}}{\partial t} = D_b^*\frac{\partial^2 c_{b0}}{\partial x^2} - Da\cdot c_{c0}c_{b0} \tag{24}$$

$$\frac{\partial c_{c0}}{\partial t} = D_P^*\frac{\partial^2 c_{c0}}{\partial x^2} - Da_{dep}\cdot c_{c0} \tag{25}$$

The initial and boundary conditions for the above equations are:

$$c_a(x,0) = c_c(x,0) = 0, \quad c_b(x,0) = c_{b0} \tag{26}$$

$$c_a(-t,t) = c_{a0}, \quad c_b(-t,t) = 0, \quad c_c(-t,t) = c_{c0} \tag{27}$$

$$c_a(Pe-t,t) = c_c(Pe-t,t) = 0, \quad c_b(Pe-t,t) = c_{b0} \tag{28}$$

Obviously, only Eq. (25) has an analytical solution; and, two other Eqs. (23) and (24) must be solved numerically. The solution for the nano-catalyst base state can be obtained using the separation of variable method, as given by Kreyszig [53]:

$$c_c(x,t) = \frac{c_{c0}}{e^{-2\sqrt{\frac{Da_{dep}}{D_P^*}}(Pe-t)}e^{-\sqrt{\frac{Da_{dep}}{D_P^*}}t} - e^{\sqrt{\frac{Da_{dep}}{D_P^*}}t}}\left(e^{-\sqrt{\frac{Da_{dep}}{D_P^*}}x} - e^{-2\sqrt{\frac{Da_{dep}}{D_P^*}}(Pe-t)}e^{\sqrt{\frac{Da_{dep}}{D_P^*}}x}\right) + \sum_{n=1}^{\infty}A_n\left(\sin\left(\frac{n\pi}{Pe}x\right) + \frac{\sin\left(\frac{n\pi}{Pe}t\right)}{\cos\left(\frac{n\pi}{Pe}t\right)}\cos\left(\frac{n\pi}{Pe}x\right)\right)e^{-\left(\frac{D_P^*n^2\pi^2}{Pe^2} + Da_{dep}\right)t} \tag{29}$$

where A_n is given by:

$$A_n = -\frac{2n\pi c_{c0}}{Pe^2\left(1 - e^{-2\sqrt{\frac{Da_{dep}}{D_P^*}}Pe}\right)\left(\frac{Da_{dep}}{D_P^*} + \frac{n^2\pi^2}{Pe^2}\right)}\left[\left(e^{-2\sqrt{\frac{Da_{dep}}{D_P^*}}Pe} - 1\right) - 2(-1)^n e^{-\sqrt{\frac{Da_{dep}}{D_P^*}}Pe}\right] \tag{30}$$

Fig. 2 illustrates different concentration profiles for fluids a, b and nanoparticles c. Time t_0 represents the corresponding times of the concentration profile. As shown in the figure, a and c have descending profiles from the injection line to the downstream domain, while b has an ascending trend. The Damköhler number usually slightly affects the concentration profile in this study, as the amounts of the nano-catalyst concentration are assumed to be very small. It is clear that the profiles are extended downstream over time. The porous medium is fully occupied by fluid b when time is close to zero. In fact, this means that fluid a and nanoparticle c appear only at the left boundary when time is exactly zero. Consequently, the introduced perturbations may be only placed in fluid b

3. Linear stability analysis

3.1. Linearized equations

We examine the linear stability of the flow to determine the effects of nanoparticle presence in the porous medium on the stability of reactive fronts. In order to linearize the problem, Eqs. (17)–(22) are substituted into Eqs. (12)–(16), and the second-order perturbation terms are eliminated from the system of equations. Eqs. (14)–(16) can be simplified further to obtain the following equations:

$$(c_a')_t + u'(c_{a0})_x = \nabla^2 c_a' + Da(c_{c0}c_b' + c_{b0}c_c') \tag{31}$$

$$(c_b')_t + u'(c_{b0})_x = D_b^*\nabla^2 c_b' - Da(c_{c0}c_b' + c_{b0}c_c') \tag{32}$$

$$(c_c')_t + u'(c_{c0})_x = D_P^*\nabla^2 c_c' - Da_{dep}c_c' \tag{33}$$

Taking the curl of Darcy's equation (12) reformulates the equation to:

$$\nabla^2 u' = K_0^{-1}(K')_{yy} - \mu_0^{-1}(\mu')_{yy} + \left[(K_0^{-1}(K_0)_x - \mu_0^{-1}(\mu_0)_x)\right](u')_x \tag{34}$$

As the coefficients of the above equations are independent of the y-direction, we may use the Fourier decomposition modes in that direction. We also implement the quasi steady-state approximation (QSSA) used by Tan and Homsy [36]. In the above formulation, the base state is a function of both time (t) and space (x). In order to use the standard linear stability analysis approach, the time dependence of the base state is eliminated using the QSSA. Using this approximation, one assumes that the small perturbations' change in time is much faster than that of the base state, allowing for the treatment of the base state as if it were steady by freezing it at one time:

$$(u', c_a', c_b', c_c') = (\xi, \psi_a, \psi_b, \psi_c)(x)e^{iky+\omega(t_0)t} \tag{35}$$

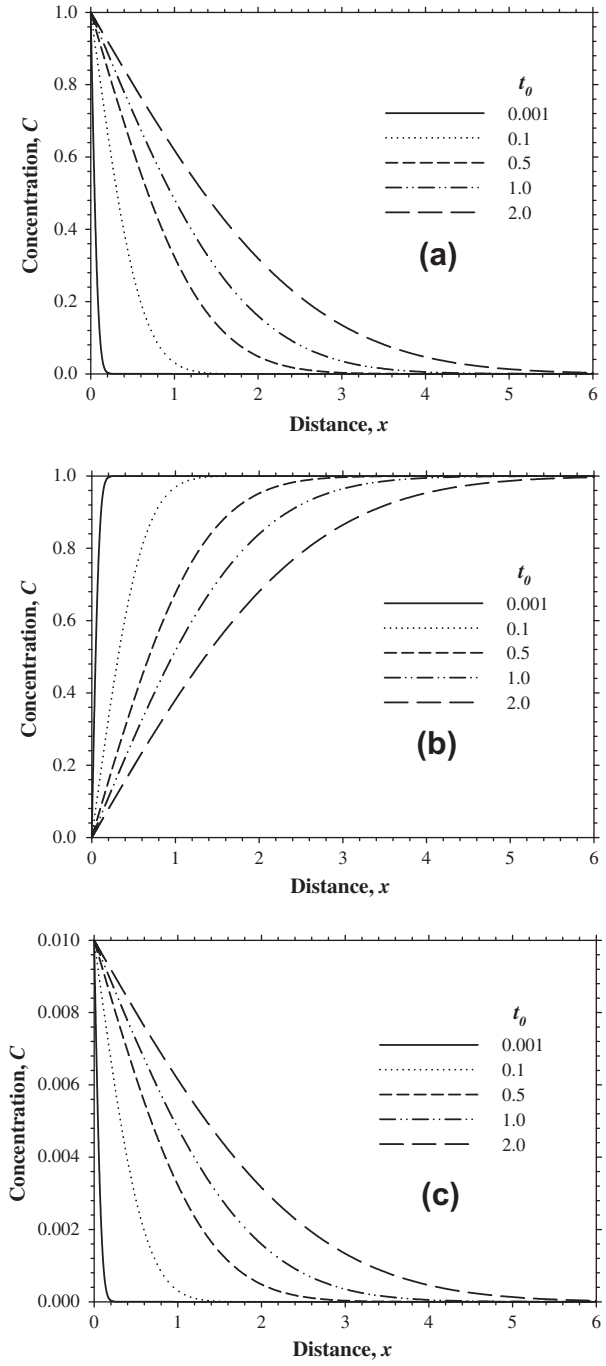

Fig. 2. Concentration profiles for *a*, *b*, *c* at different times, $Da = 0$, $Pe = 1500$, $D_P^* = 1$, $Da_{dep} = 0.01$.

where k and ω are the wavenumber and growth rate of the perturbations, respectively; and time t_0 is also frozen time. Substituting Eq. (35) into Eqs. (31)–(34), one can obtain:

$$(\psi_a)_{xx} - \left(k^2 + \omega\right)\psi_a = \xi(c_{a0})_x - Da(c_{b0}\psi_c + c_{c0}\psi_b) \tag{36}$$

$$D_b^*(\psi_b)_{xx} - \left(k^2 D_b^* + \omega + Da \cdot c_{c0}\right)\psi_b = \xi(c_{b0})_x + Da \cdot c_{b0}\psi_c \tag{37}$$

$$D_P^*(\psi_c)_{xx} - (k^2 D_P^* + Da_{dep} + \omega)\psi_c = \xi(c_{c0})_x \tag{38}$$

$$(\xi)_{xx} - \left[\beta(c_{c0})_x - \alpha_a(c_{a0})_x - \alpha_b(c_{b0})_x - \alpha_c(c_{c0})_x\right]\xi_x - k^2\xi = \alpha_a k^2\psi_a + \alpha_b k^2\psi_b + \left(\alpha_c k^2 - \beta k^2\right)\psi_c \tag{39}$$

The boundary conditions that are required to solve the system of equations are:

$$\psi_a = \psi_b = \psi_c = \xi = 0 \text{ at } x = -t \text{ and } x = Pe - t \tag{40}$$

Eq. (40) implies that the boundaries remain unperturbed. The above system of Eqs. (36)–(40) is an eigenvalue problem where we may find the growth rate, ω, for each wavenumber, k, using a numerical approach. A finite difference method is used to solve the eigenvalue problem consisting of a system of four coupled ordinary differential equations. The finite difference technique has advantage over other methods, since by using this method the complete spectrum of the eigenvalues can be obtained. The spatial derivatives are approximated using second-order central difference formula. A non-uniform geometric mesh is used which is very fine around the interface where the concentration gradients are large, and spacing increases geometrically with the distance from the origin. Eigenfunctions are discretized using this technique, and the computation domain is chosen wide enough to capture all the eigen-solutions. A standard method is used to solve for the eigenvalues and eigenvectors of the resulting problem. In this approach reduces the general real matrix into an upper Hessenberg form in order to solve for the eigenvalues. In order to check the validity of the results, the code was tested for a domain size of 100, 200 and 300. The results were reported if the convergence was achieved quickly and the obtained results were the same for all number of meshes with the appropriate geometric spacing. The discrete eigenvalues are insensitive to the width of the domain, if the domain is chosen large enough to accommodate the decaying eigenfunctions. From the set of discrete eigenvalues obtained, we report only the largest one, since for given values of the parameters it dominates all other modes.

4. Results and discussion

In this section, the dispersion curves for different scenarios are plotted and examined. It is necessary to mention that, in all cases, the logarithmic viscosity ratios ($\alpha_a = -3$, $\alpha_b = 0$, $\alpha_c = 0$), logarithmic permeability ratio ($\beta = -2$), frozen time ($t_0 = 2$), nanoparticle diffusion coefficient ($D_P^* = 1$), fluid diffusion coefficient ($D_b^* = 1$), reaction rates ($Da = 2$, $Da = 10$), and nano-catalyst concentrations ($c_{c0} = 0.01$, $c_{c0} = 0.002$) are all considered to be constant, unless the sensitivity of these parameters is being studied.

In our examination, the variation of growth rates with wavenumbers is discussed for different nano-catalyst concentrations and Damköhler numbers. We first discuss a simplified case, for which the numerical results can be validated. It is necessary to mention that this parametric study is not universal, as we always need to assume some parameters are fixed.

4.1. Special case

In order to validate the developed numerical code, some special cases are studied. First, it is assumed that the nano-catalyst concentration in the medium is zero, so that no reaction takes place. This results in a simple displacement where instability may occur, due to the viscosity difference between the displacing and the displaced fluids. The time, t_0, is assumed to be zero, so that a step function profile can be found for fluids *a* and *b*.

It should be mentioned that the step function solution ($t_0 = 0$) is different from the classic work of Tan and Homsy [36]. They had the miscible interface at the middle of geometry and found that the step function always results in the most unstable growth rate. However, as we are dealing with an unperturbed boundary layer problem (see Fig. 2), the flow system could be totally stable. Their results may be recoverable, if we deal with a perturbed boundary layer instead. In fact, in the classic works of viscous fingering

[22,23,35,36], the introduced perturbations are placed in both fluids *a* and *b* on the left- and right-hand sides of interface. Using a jump condition, this could result in an analytical solution.

In our study, however, the step function profile results in a system in which perturbations are placed in only fluid *b*, right after the injection line. In this case, fluid *b* is only in contact with fluid *a* and nanoparticle *c* at the boundary. In this scenario, the jump condition cannot be valid, as the boundary is assumed to be unperturbed. In this case, we need only to solve Eqs. (36)–(40) for component *a*. The simplified equations are given by:

$$(\psi_a)_{xx} - (k^2 + \omega)\psi_a = \xi(c_{a0})_x \tag{41}$$

$$(\xi)_{xx} + \left[\alpha_a(c_{a0})_x\right]\xi_x - k^2\xi = \alpha_a k^2 \psi_a \tag{42}$$

Since the boundary remains unperturbed, as shown in Eq. (40), the base state solution is a step function when t_0 has a very small value. Consequently, an analytical solution can be obtained for Eq. (41) when $x > 0$:

$$\psi_a(x) = A_1 \exp\left(-\sqrt{k^2 + \omega}x\right) + A_2 \exp\left(\sqrt{k^2 + \omega}x\right) \tag{43}$$

Implementing the appropriate boundary conditions (40) gives:

$$A_1\left(1 - \exp\left(2\sqrt{k^2 + \omega}Pe\right)\right) = 0 \tag{44}$$

$A_1 = 0$ results in $A_2 = 0$; thus, $\psi_c = 0$. As the eigenfunctions should be non-zero, the growth rate can be found easily from Eq. (44):

$$\omega = -k^2 \tag{45}$$

Indeed, the solution reveals that the system is totally stable for a step function profile of *a*, *b* and *c*. In this scenario, perturbations are located in a uniform profile of fluid *b* and are damped, while the boundary remains unperturbed. Although there is a viscosity difference between the displacing and displaced fluids, the system remains stable at short times. Consequently, in order to destabilize the front, a viscosity profile between the fluids has to be established as time passes. However, the flow system gradually turns unstable as t_0 increases. In fact, the diffusion of components *a* and *c* from the left boundary into the flow system causes a viscosity profile to be established. Consequently, there is enough driving force for perturbations to grow.

Fig. 3 compares the analytical solution (Eq. (45)) with numerical ones for a non-reactive flow system ($c_{c0} = 0$). It can be observed that the numerical solutions gradually overshadow the analytical one (the solid thick line), if t_0 is short enough.

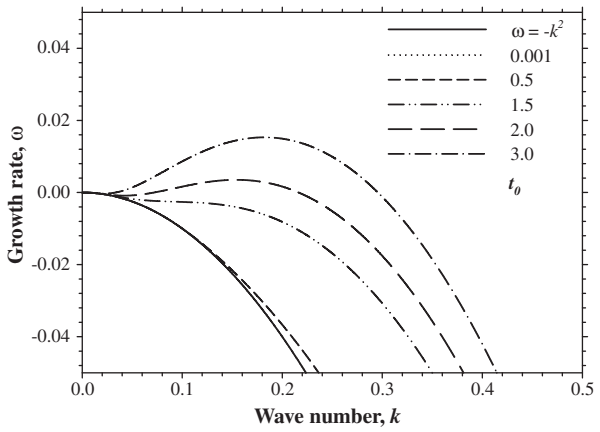

Fig. 3. Variation of wavenumber versus growth rate for a non-reactive flow system, $c_{c0} = 0$, $Da_{dep} = 0.01$, $D_p^* = 1$.

4.2. Parametric studies

The effects of viscosity difference and different types of non-catalytic chemical reactions on the fingering instability have been extensively studied in the past decades [22,23,26,35,36]. These studies have revealed that increasing the adverse viscosity ratio or rate of chemical reaction in a miscible displacement mainly results in a larger maximum growth rate, which means a more unstable flow system. However, it is still unknown how this hydrodynamic instability may be affected when the displacing phase carries nanoparticles. The addition of nanoparticles to liquids usually increases the viscosity of a solution [54].

The role of nanoparticle addition and flow of these particles in porous media on any kind of fingering instability is unknown, especially when these particles are used as catalysts to drive a chemical reaction. In this section, an attempt is made to reveal how the addition of only small amounts of nanoparticles can affect fingering instability. As the effects of viscosity ratios and general non-catalytic chemical reaction are well known in the literature [22], the focus in this study is more on the role of nanoparticles. The concentration of nanoparticles and its impact on the chemical reaction, rate of deposition and molecular diffusion coefficient of these particles are discussed in detail.

It is necessary to mention that the growth or damping of the perturbations depends on three competing mechanisms of mass transportation, including hydrodynamic convection, fluid and nanoparticle diffusion, and reaction chemistry. Perturbations may grow by one or two of the mechanisms, while damping occurs by the other one(s). In fact, different scenarios may be found, depending on the physics of the problem. In what follows, the effects of different physical parameters are discussed further.

4.2.1. Effect of front sharpness

Hydrodynamic and fingering instability has been known to be highly affected by the concentration profiles of different components in a miscible displacement [22,36]. The profile can usually be extended downstream by changing the frozen time. As time increases, more amounts of displacing phase *a* and nano-catalysts *c* may diffuse into host fluid *b* in a porous medium. At the same time, the reactant and product (*b* and *a*) concentration profiles are directly related to the nano-catalyst concentration profile (see Eqs. (14)–(16)).

To determine how the sharpness of the front affects the instability, especially maximum growth rates and cutoff wavenumbers, dispersion curves are plotted for a series of t_0 at two different Damköhler numbers. Fig. 4 reveals that the range of unstable spectrum wavenumbers is initially shifted to larger values for both reaction rates ($Da = 2$ and $Da = 10$) when t_0 increases. Indeed, the boundary layer turns out to be completely unstable as it becomes more diffusive. Time $t_0 = 10$ seems to be a turning point in both cases ($Da = 2$ and $Da = 10$). Diffusion plays a destabilizing role for times shorter than 10, while it has a stabilizing role for longer times.

Diffusion and convection, as well as chemical reaction, are the main mechanisms that are competing here to drive instability. In fact, diffusion initially helps to establish the viscosity gradient as the main source of fingering instability; however, viscosity profile becomes established beyond the injection line. This can be the reason why cutoff wavenumbers are initially moving towards the larger numbers and diffusion plays a destabilizing role. However, as diffusion time increases, the concentration field and, in turn, the viscosity profile becomes relatively more uniform; and, the flow system is less unstable. The same behavior may be observed when the nano-catalyst concentration is low ($c_{c0} = 0.002$); however, the

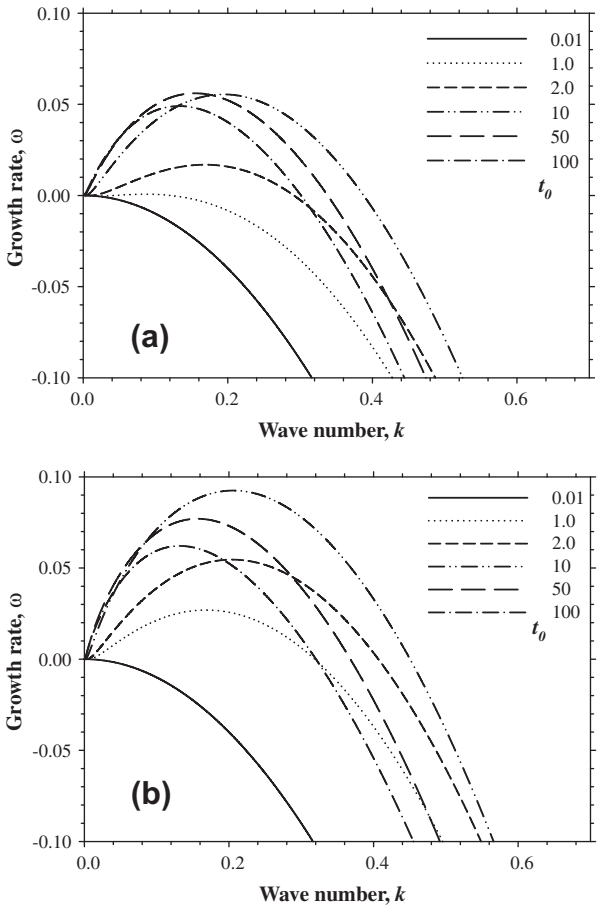

Fig. 4. Dispersion curves for different t_0: (a) $c_{c0} = 0.01$, $Da = 2$; (b) $c_{c0} = 0.01$, $Da = 10$, $Da_{dep} = 0.01$.

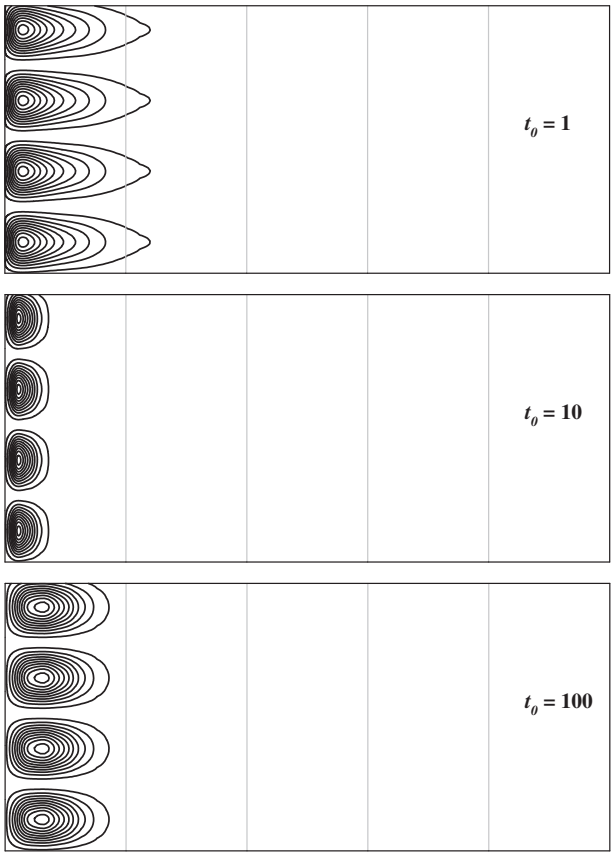

Fig. 5. Contours of streamlines for three different t_0; $c_{c0} = 0.01$, $k = 0.2$, $Da = 10$, $Da_{dep} = 0.01$, $D_p^* = 1$.

stabilizing effect of diffusion appears at shorter times, in comparison with higher concentrations of nano-catalysts. The same explanation is applicable here; and, it is attributed to the establishment of the viscosity profile, which is the driving force for the fingering instability here.

More physical illustrations may be presented by the streamline contours for $Da = 10$ and a wavenumber equal to 0.2, where the flow system is unstable for all scenarios. The perturbations and the base state distribution of all three components play a major role in the determination of the degree of stability or instability of a flow system. Here, the streamlines are all normalized between zero to one. In fact, streamline contours correspond to the area in which the mixing between low and high viscosity fluids is effective.

Fig. 5 depicts that mixing is extended more downstream from the injection line for $t_0 = 1$ than for other cases; whereas, it is more compact for $t_0 = 10$, which is the most unstable case. Indeed, this reveals that mixing between low and high viscosity fluids is higher for short times, which results in a more uniform viscosity profile along the domain. Consequently, one may expect a less unstable flow system when t_0 is adequately short ($t_0 = 1$) or long ($t_0 = 100$), in comparison with an average time ($t_0 = 10$). This figure can also clearly depicts why the flow system at $t_0 = 1$ is less unstable than at $t_0 = 100$.

4.2.2. Effect of reaction rate

As shown in Eq. (2) and explained by Levenspiel [46], for homogeneous catalytic reactions, nano-catalysts only affect the kinetics of the chemical reaction, but their concentration remains unchanged when the chemical reaction takes place. The concentration profiles of the reactant (a) and product (b) are slightly affected by nano-catalysts at different Damköhler numbers, as the nano-catalyst concentration is assumed to be low.

Basically, the analytical and numerical results describe the base state concentration profiles; thus, the viscosity profiles are slightly varied by either the nano-catalyst concentration or the Damköhler number. In fact, the trend of the base state concentration profile is mainly controlled by convection and diffusion and not by reaction chemistry in the current study, as the range of nanoparticle concentrations is very low ($c_{c0} < 0.01$).

Fig. 6, however, clearly shows that the chemical reaction rate could dramatically shift the flow system towards more unstable systems. The figure represents results for different Damköhler numbers. In most of the scenarios, the flow systems are stable at small and large enough wavenumbers. Two different nano-catalysts concentrations have been assigned to the curves. In particular, one may notice how introducing a reaction at the interface around the injection line can increase the fingering instability of the front of a non-reactive system. It can be also seen that the dispersion curves are significantly shifted to a larger spectrum of wavenumbers as the nano-catalyst concentration varies.

It should be mentioned that the argument that the flow should be more stable when the reaction rate increases, as more fluids with less viscosity are produced, is not valid here. First, the interface remains relatively unchanged. Second, the base state concentration profile becomes slightly more diffusive when the Damköhler number increases. In particular, based on our discussion regarding the effect of t_0, one may expect a more unstable system when the Damköhler number increases. In fact, more fluid of lower viscosity is transferred from the highly viscous side of the interface to the less

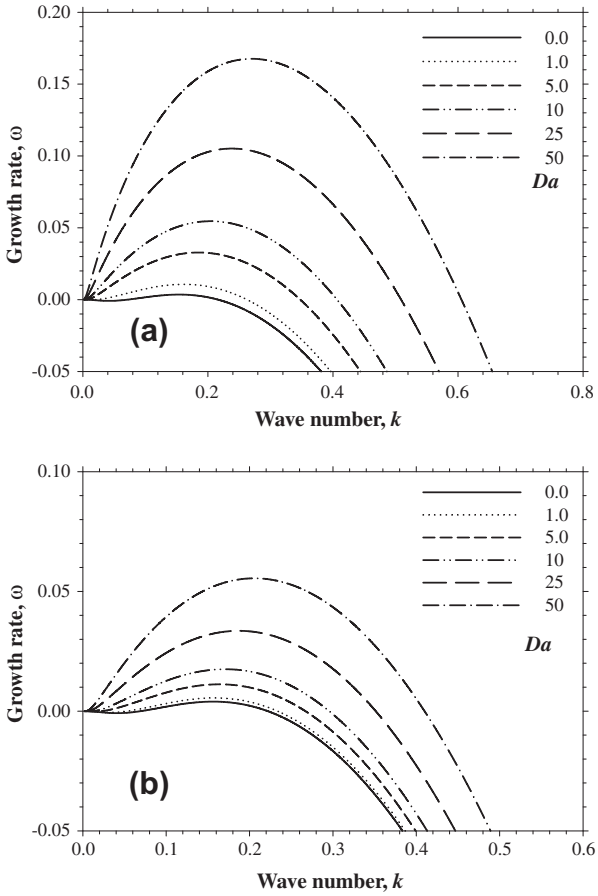

Fig. 6. Dispersion curves for different Damkohler numbers: (a) $c_{c0} = 0.01$; (b) $c_{c0} = 0.002$.

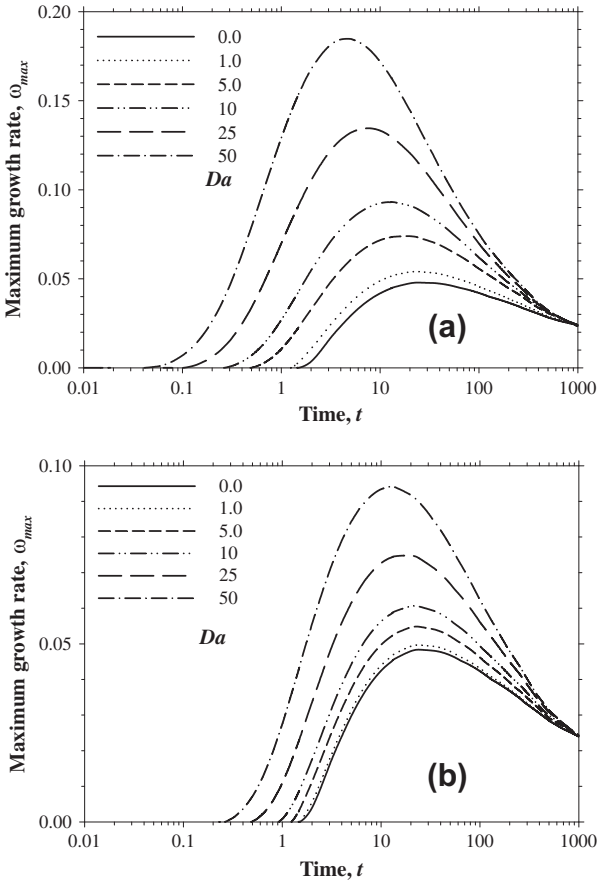

Fig. 7. Variation of maximum growth rate with time at two different nanoparticle concentrations, $D_p^* = 1$, $Da_{dep} = 0.01$ (a) $c_{c0} = 0.01$; (b) $c_{c0} = 0.002$.

viscous one; however, the base state profile is shifted towards a more diffusive pattern. This may, in turn, increase the instability. As the base state concentration profile change is small, one may look for a stronger illustration using perturbation effects. Consequently, the distribution and role of perturbations is the key in elucidating the trend of maximum growth rate/wavenumber variation at different Damköhler numbers. In general, perturbations should describe how the instability may vary with chemical reactions.

The analyses of Fig. 6 for different concentrations ($c_{c0} = 0.01$ and $c_{c0} = 0.002$) reveals that chemistry drives instability. As the effect of nano-catalyst concentration on the fingering instability aligns with the chemical reaction rate (Da), a detailed examination of how the perturbations impact the fingering instability for such a system is presented in more detail in the next section.

It is shown that increasing t_0 or making the interface more diffusive initially has a destabilizing effect, but has a stabilizing effect later on. More analysis is conducted to reveal how t_0 and Damköhler number together may affect the flow system. Fig. 7 depicts the variation of the most unstable growth rate with time at different Damköhler numbers for two concentrations ($c_{c0} = 0.01$ and $c_{c0} = 0.002$). It can be seen that flow systems with a larger reaction rate are always more unstable at different times. This supports our previous discussion that a more intensive chemical reaction always makes the system more unstable.

As shown in Fig. 7, at all Damköhler numbers, the flow system initially becomes more unstable as time goes by; however; it becomes less unstable after reaching its extrema. The same physical interpretation as discussed before may be recalled here to justify how the flow system is initially destabilized and then stabilizes.

Two significant findings should be mentioned here. First, the instantaneous growth rate variation with time reveals that a flow system with a higher concentration of nano-catalysts is destabilized at shorter times than a system with a smaller concentration. Second, the instantaneous growth rates for all Damköhler numbers are merged into a unique value at very long times. This means that, when fluids a and b are adequately mixed at long times, chemical reaction and diffusion are not effective mechanisms in driving the instability, compared to the viscous forces.

Fig. 8 depicts the onset time of instability at different reaction rates and nanoparticle concentrations. The flow system begins to be unstable at longer times as the concentration of nanoparticles is decreased in a porous medium. The onset time initially descends sharply with the Damköhler number. It is clear that the onset time seems independent of the reaction rate at high enough Damköhler numbers.

4.2.3. Effects of nano-catalyst concentration

Nanoparticles are usually used in low concentrations in porous media; however, the concentration may increase or decrease around the front for reasons such as accumulation, deposition or aggregation. The nano-catalyst concentration may also influence the reaction speed, which can result in different concentration profiles for reactants and products. In fact, this represents the complexity of the nano-catalyst concentration role in porous media. It has been already shown that a less intensive chemical reaction, which could even correspond to a reduced concentration of nano-catalysts, shifts the flow system to smaller cutoff wavenumbers and growth rates; however; the trend of dispersion curves remain the same.

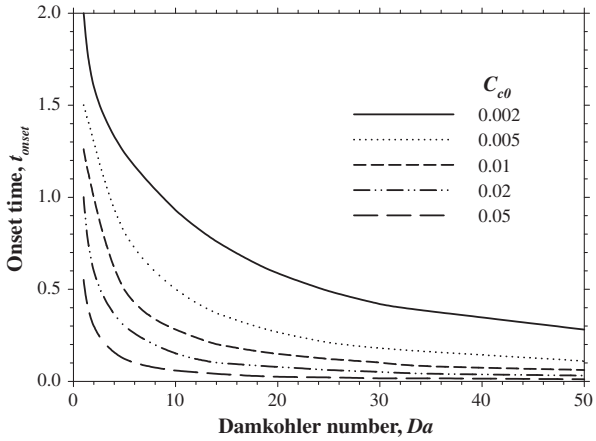

Fig. 8. Variation of the onset time of instability with reaction rate at different nano-catalyst concentrations, $Da_{dep} = 0.01$, $D_p^* = 1$.

We now examine how the nano-catalyst concentration changes the dispersion curves. The effect of this concentration in the displacing phase on the stability of the front is illustrated in Fig. 9 for two different Damköhler numbers ($Da = 2$ and $Da = 10$). As shown, the flow system is less unstable when the nano-catalysts concentration is very small ($c_{c0} = 0.001$). However, the front can become more unstable as the nano-catalyst injection concentration increases, so that the flow system becomes highly unstable for $c_{c0} = 0.1$. Indeed, Fig. 9 shows how the concentration of nanoparticles may affect the hydrodynamic stability of the front.

As previously mentioned, the reason why the faster chemical reactions originate from either larger Damköhler numbers or higher concentrations of nano-catalysts may be sought in the perturbation effects on the instability. Clearly, two main mechanisms are competing here to drive instability. First, the chemical reaction, which becomes more intensive by increasing nano-catalysts concentration, has already been shown to have a destabilizing impact.

Second, viscous forces are weakened by an increase in nano-catalyst concentration. In fact, the viscosity of the displacing phase increases; and, in turn, the viscosity difference between the two phases decreases. However, one may consider this effect to still be negligible when the concentration of nano-catalysts is one or two orders of magnitude smaller than fluids *a* and *b*. At the same time, the logarithmic mobility ratio for nanoparticles is smaller in comparison with fluids *a* and *b*. In fact, Fig. 9 illustrates that the chemical reaction effects are stronger here and more pronounced on the front instability.

As previously discussed, the instability increase by chemical reaction may be explained by the key role of perturbation, as the base state profile varies slightly with an increment in the reaction rate of the nanoparticle concentration. To elucidate the effects of the chemical reaction and the nano-catalyst concentration on the instability, we again plot the contours of normalized streamlines.

Fig. 10 represents the normalized streamlines in two dimensions, where both the nano-catalyst concentration (from top to the bottom) and the Damköhler number (left to right) are increasing. Basically, these contours represent the fluid circulation right after the injection line, where less viscous fluid is brought into contact with the higher viscous one and mixing occurs. It is clear that the contours become wider as either the concentration behind the injection line or Damköhler number decreases.

At the same time, the center of the vortices is shifted downstream. Consequently, the flow circulation covers a wider range in the domain, leading to the mixing of fluids of less viscosity with higher ones, when either the nano-catalyst concentration or Damköhler number is small. This, in turn, results in a more stabilized system.

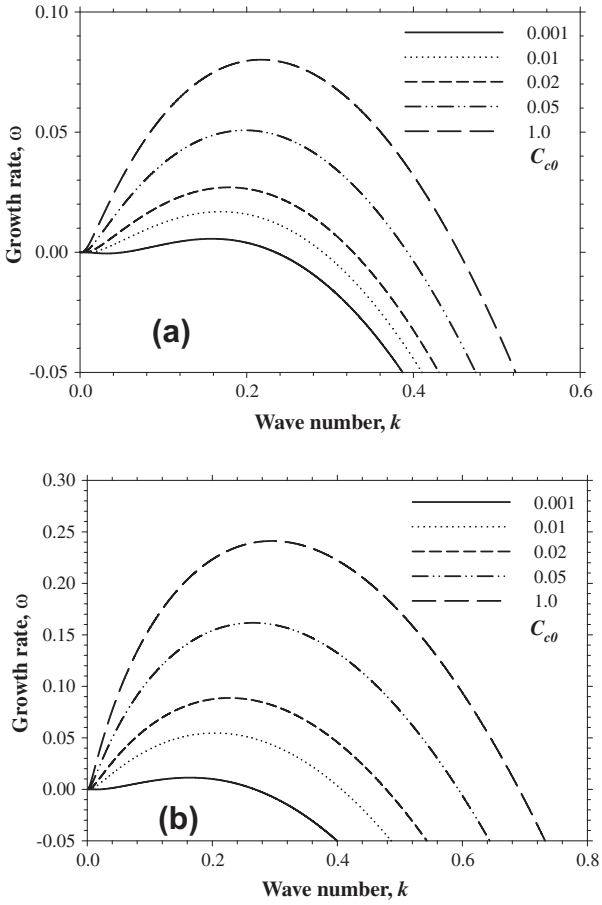

Fig. 9. Dispersion curves for different concentration of nano-catalysts, $Da_{dep} = 0.01$, $D_p^* = 1$: (a) $Da = 2$; (b) $Da = 10$.

It can be concluded here that the flow system becomes more unstable with any change resulting in a faster reaction. In fact, the flow circulation and vortices and also the center of the vortices are extended upstream with any change, which makes the reaction more intensive, by either increasing the Damkohler number or the nano-catalyst concentration.

For given values of the deposition rate ($Da_{dep} = 0.01$), frozen time ($t_0 = 2$) and nanoparticle diffusion coefficient ($D_p^* = 1$), the contours of the maximum growth rates can be determined. Fig. 11 illustrates the maximum growth rate contours for different nano-catalyst concentrations and chemical reaction rates. From Fig. 11 and based on our discussion, one should expect that the most unstable flow system when both the nano-catalyst concentration and the Damkohler number are large. This also reveals that variation of the instantaneous growth rate with respect to the nano-catalyst concentration and Damköhler number is more pronounced when either the concentration or Damköhler number is small.

4.2.4. Effect of nanoparticle diffusion coefficient

The diffusion coefficient is another physical property of nanoparticles that has a significant role in their applicability in porous media. The order of magnitude of the diffusion coefficient may be the same as that of the carrier fluid; however, it may vary depending on the type of particles. Although there is still a lack of knowledge in the measurement of the diffusion coefficient of nanoparticles in gas and liquids, especially in saturated porous media, there have been recent attempts to measure the coefficient [55,56].

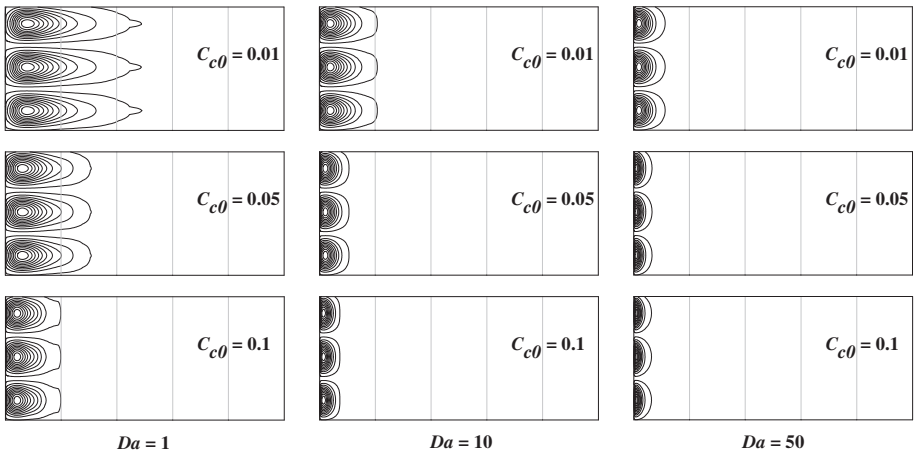

Fig. 10. Streamline contours for different nano-catalysts concentrations and Damkohler numbers, $k = 0.15$, $t_0 = 2$, $Da_{dep} = 0.01$, $D_p^* = 1$.

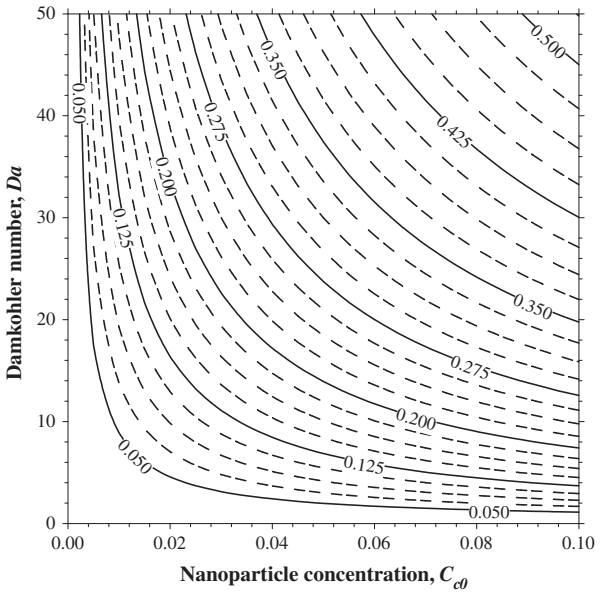

Fig. 11. Contours of the maximum growth rates for different nanoparticle concentrations and Damkohler numbers.

One may find that nanoparticle diffusion coefficients can be a function of different parameters, such as particle size, material base and temperature. A wide range of diffusion coefficients from the order of 10^{-5} to 10^{-11} m^2/s have been reported by Rudyak et al. [55] and d'Orlyé et al. [56]. Consequently, the nanoparticle to liquid diffusion coefficients suggest various ratios, depending on the fluid type – from water to very viscous liquids, such as heavy oil and polymer solutions.

As shown by Einstein [57], the particle size and diffusion coefficient are inversely proportional, so that any variation in the instability trend with the diffusion coefficient may also be considered as the effect of the nanoparticle size. The relationship is valid for particles with Brownian motion, where the diffusion coefficient of the particles is proportional to the inverse of particle size so that $\left(D_P^* \approx d_p^{-1}\right)$. Assuming that Einstein's relationship is valid here, one may relate the impact of the nanoparticle diffusion coefficient on the reactive front stability to the particle size, if small particles represent a large diffusion coefficient and vice versa.To study the effect of nanoparticle diffusion coefficients or nanoparticle size on the stability of reactive fronts, we first consider a special case in which the nanoparticle diffusion coefficient is zero. The system of Eqs. (36)–(40) can mathematically have a general solution, where the particle diffusion coefficient D_P^* will be approximately zero; in other words, the only mechanism of mass transportation in the flow system for the nanoparticles is convection. In this case, the nano-catalyst base state has a step function distribution in the domain. This, in turn, further simplifies the nano-catalysts mass conservation equation (Eq. (38)) to:

$$-(Da_{dep} + \omega)\psi_c = \xi(c_{c0})_x \tag{46}$$

The derivative of the nano-catalyst base is zero everywhere in the domain. Since the eigenfunctions, ψ_a, ψ_b, ψ_c and ξ, should have non-zero values, two possible cases may be considered: either $\omega = -Da_{dep}$ or $\psi_c = 0$, but ψ_a, ψ_b and ξ may be nonzero. The first case results in a stable flow system, in which the growth rate is the negative of the deposition rate constant. In the second case, the set of Eqs. (36)–(39) can be analyzed.

$$(\psi_a)_{xx} - (k^2 + \omega)\psi_a = \xi(c_{a0})_x \tag{47}$$

$$(\psi_b)_{xx} - (k^2 + \omega)\psi_b = \xi(c_{b0})_x \tag{48}$$

$$(\xi)_{xx} - [\beta(c_{c0})_x - \alpha_a(c_{a0})_x - \alpha_b(c_{b0})_x]\xi_x - k^2\xi = \alpha_a k^2\psi_a + \alpha_b k^2\psi_b \tag{49}$$

When a short t_0 is considered, a and b base states can have also a step function form for a sufficiently small value of t_0. Assuming step function profiles for all three base states suggests a simpler set of equations than Eqs. (47)–(49). The equations convert to Eqs. (41) and (42) and have non-zero eigenfunctions of ψ_a, ψ_b, and ξ; and, the solution is:

$$\omega = -k^2 \tag{50}$$

In fact, this indicates that the flow system, including nano-catalysts, is always stable for a zero nanoparticle diffusion coefficient at short times, as the growth rate is negative. It can be concluded that the corresponding growth rate of each wavenumber is a combination of both $\omega = -Da_{dep}$ and $\omega = -k^2$ curves.

In order to check the validity, results for different values of particle diffusion coefficients are now tested numerically. Fig. 12a clearly depicts the analytical trend, showing the dispersion curves for $Da_{dep} = 0.01$ and different nanoparticle diffusion coefficients. The growth rate for a large particle diffusion coefficient decreases sharply and the flow system is always stable, however; it converges into a plateau at -0.2 when the nanoparticle diffusion coefficient is becoming zero $(D_P^* = 0)$, as shown by the solid line in the figure.

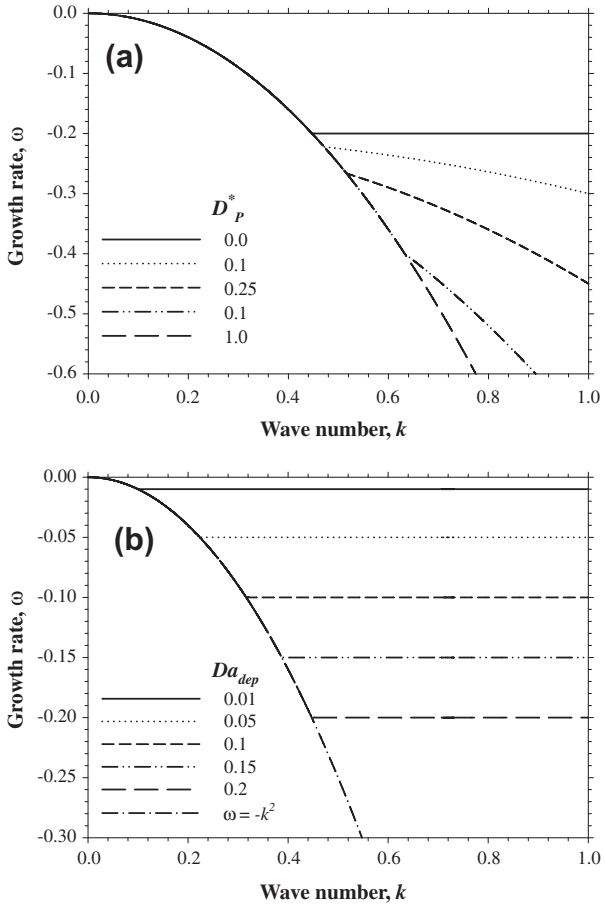

Fig. 12. Dispersion curves for $Da = 2$, $c_{c0} = 0.01$: (a) different particle diffusion coefficients and $Da_{dep} = 0.2$; (b) different deposition rates and $D^*_P = 0$.

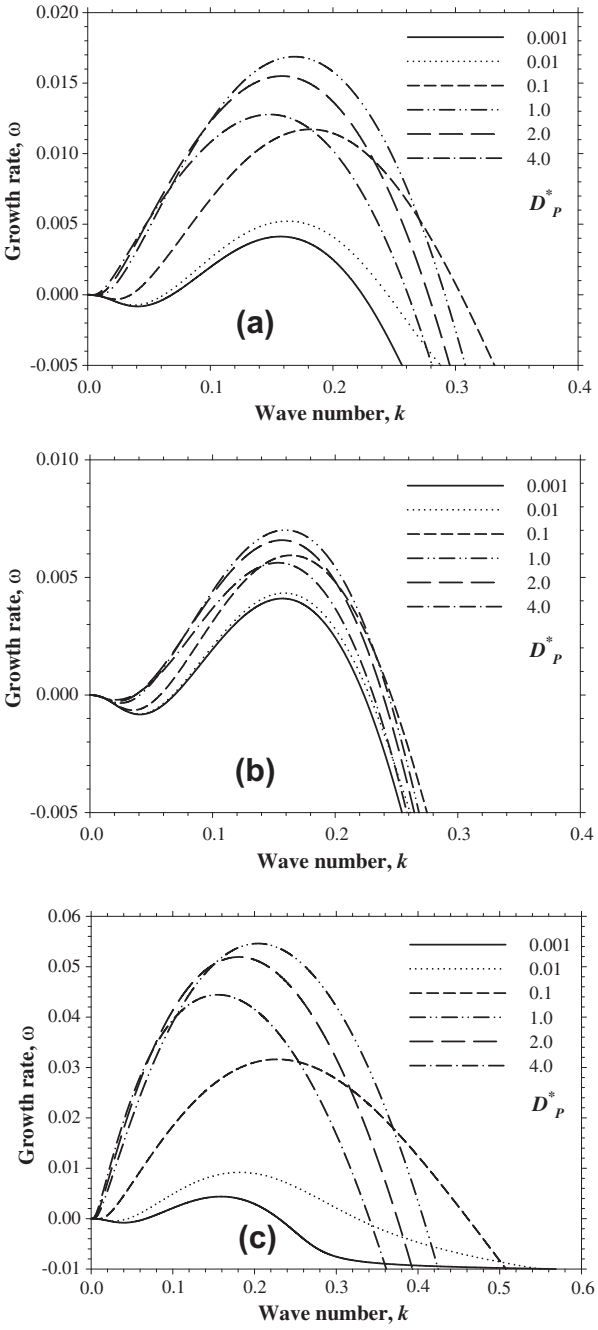

Fig. 13. Dispersion curves for different nanoparticle diffusion coefficients at $t_0 = 2$: (a) $c_{c0} = 0.01$, $Da = 2$; (b) $c_{c0} = 0.002$, $Da = 2$; (c) $c_{c0} = 0.01$, $Da = 10$.

Further investigation may be performed to check this argument. Another scenario is considered here, where the nanoparticle diffusion coefficient is zero, but different values are assigned to deposition rates. Fig. 12b clearly shows that all of the dispersion curves converge to different plateaus at the negatives of different deposition rates, and the system is stable in all cases. The growth rate for small wavenumbers follows the $\omega = -k^2$ solution, as shown by the solid line. In fact, when t_0 is short enough (i.e. $t_0 = 0.005$), the results are exactly the combination of both the $\omega = -Da_{dep}$ and $\omega = -k^2$ curves. The flow system is tested for other cases with a small nanoparticle diffusion coefficient, and all dispersion curves show the same behavior.

Fig. 13 illustrates the variation of growth rate versus wavenumbers for different nanoparticle diffusion coefficients at two different reaction rates and concentrations. It is revealed that stability of the front is dramatically affected by the nanoparticle diffusion coefficient. There is a non-monotonic trend, such that the flow system becomes more unstable as the diffusion coefficient increase, but becomes less unstable as the diffusion coefficient goes over one. A diffusion coefficient of one may be considered as the critical value in all scenarios.

Our arguments explaining the stabilization and destabilization effects of diffusion may be applied here again. Basically, the nanoparticles can move further as the diffusion coefficient increases, resulting in a more diffusive base state. This can be again attributed to the destabilization and stabilization effects of diffusion around the time of analysis, where the nanoparticle base state becomes more diffusive as the nanoparticle diffusion coefficient, D^*_p, increases. Indeed, the system is stable when the fronts are sharp enough; however, diffusion gradually plays a significant role in making the front more unstable, by expanding the reactive area.

One should recall that the flow system is stable for a non-reactive flow system with a sharp front (small t_0), but the reaction can turn that system to an unstable one as the Damköhler number increases. The same explanation can again be applied here. Indeed, the diffusion of nanoparticles can cause the expansion of the reaction zone, which has a destabilizing effect. However, the stabilizing effect of diffusion can overwhelm the competitive mechanisms and make the front more stabilized, when the mixing area is shifted downstream.

4.2.5. Effect of nano-catalyst deposition

The reactivity and mobility of nano-catalysts are the most significant parameters to determine the progress and efficiency of the reaction. In fact, nano-catalysts with a low mobility can dramatically affect the efficiency and even stop the process. In addition, a low mobility or high deposition rate of the nano-catalysts may also influence the stability of the front. The nanoparticles may aggregate and deposit into the medium as the Brownian motion of the particles and the van der Waals and repulsive forces for nano scale particles are important.

Fig. 14 indicates the dispersion curves for various nano-catalyst deposition rates at two different nano-catalyst concentrations and two Damköhler numbers. This reveals the significance of the nanoparticle deposition, even for a small particle number density in the medium, where the flow system leads to more unstable flows as the rate of nanoparticle deposition increases.

A change in the dispersion curve trends can also be realized as if the flow system is stable at very small wavenumbers when the deposition rate is large. However, negative growth rates at small wavenumbers fade away gradually as the rate of nanoparticle deposition increases. Basically, the flow system is more unstable when the mobility of nanoparticles in the pores is higher.

In general, the cutoff wavenumbers and maximum growth rates are shifted towards a larger spectrum, as the deposition rate decreases. This again may be attributed to the deposition effect on the reaction rate and the nano-catalyst concentration. It has been already argued how increasing the Damköhler number or increasing the nano-catalyst concentration can affect the stability of the flow system.

In fact, a higher deposition rate causes a reduced concentration of the nano-catalysts in the mobile phase, which can result in a slower reaction. Both the smaller nano-catalyst concentration and slower reaction have been shown earlier to have a stabilizing effect on the flow system. Basically, the same discussion can be valid here.

All scenarios show the same trend. However, it seems that the dispersion curve reaches a limiting mode ($Da_{dep} = 1$) for a low concentration case (Fig. 14b), where the reaction and deposition rate are in the same order. It can be argued that the concentration of nano-catalysts is negligible in the medium, and the reaction is very slow. Consequently, the non-reactive flow system stability analysis may be recoverable here.

The variation of instantaneous maximum growth rates with time is shown in Fig. 15, which depicts that a flow system with smaller

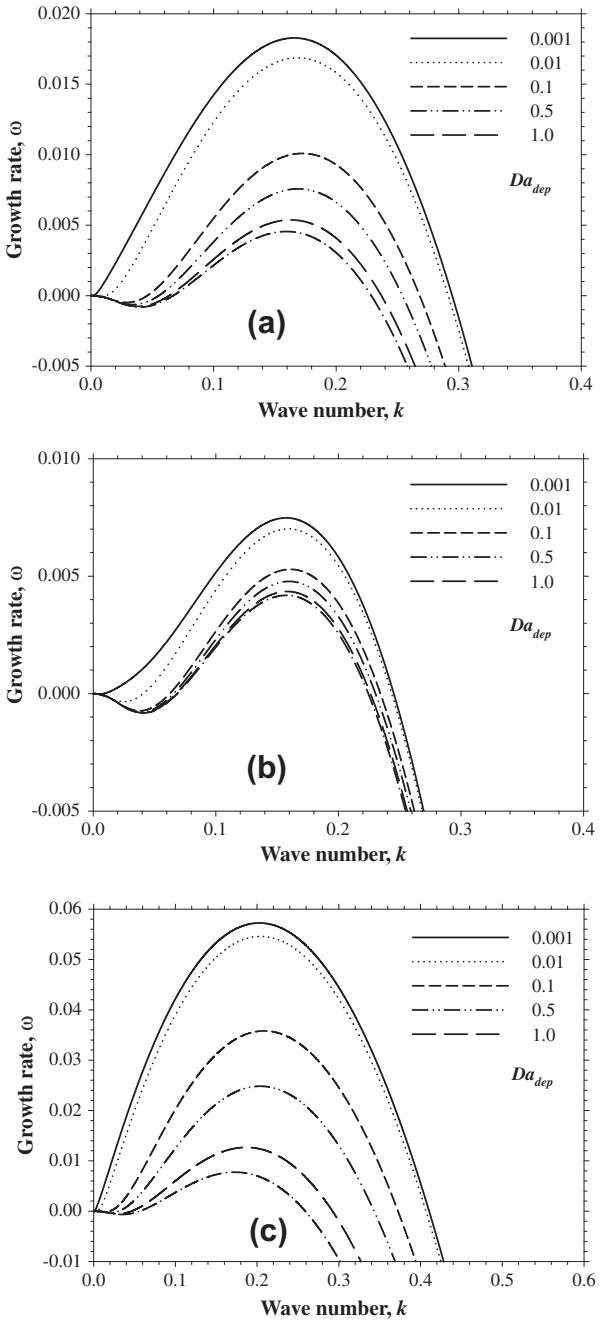

Fig. 14. Dispersion curves for different nano-catalysts deposition rates at $t_0 = 2$: (a) $c_{c0} = 0.01$, $Da = 2$; (b) $c_{c0} = 0.002$, $Da = 2$; (c) $c_{c0} = 0.01$, $Da = 10$.

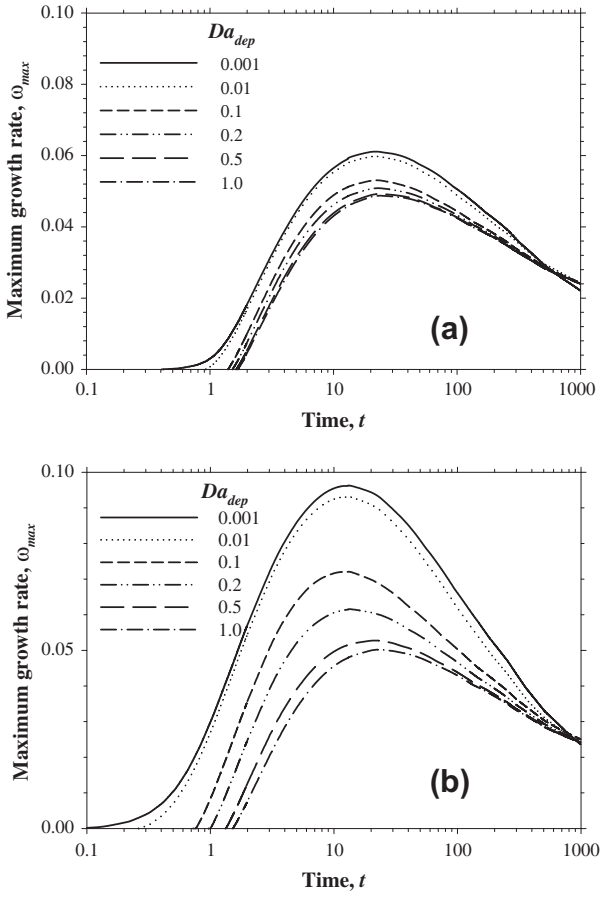

Fig. 15. Variation of maximum growth rate with time for different deposition rates, $t_0 = 2$, $c_{c0} = 0.01$, $D_p^* = 1$: (a) $Da = 2$; (b) $Da = 1$.

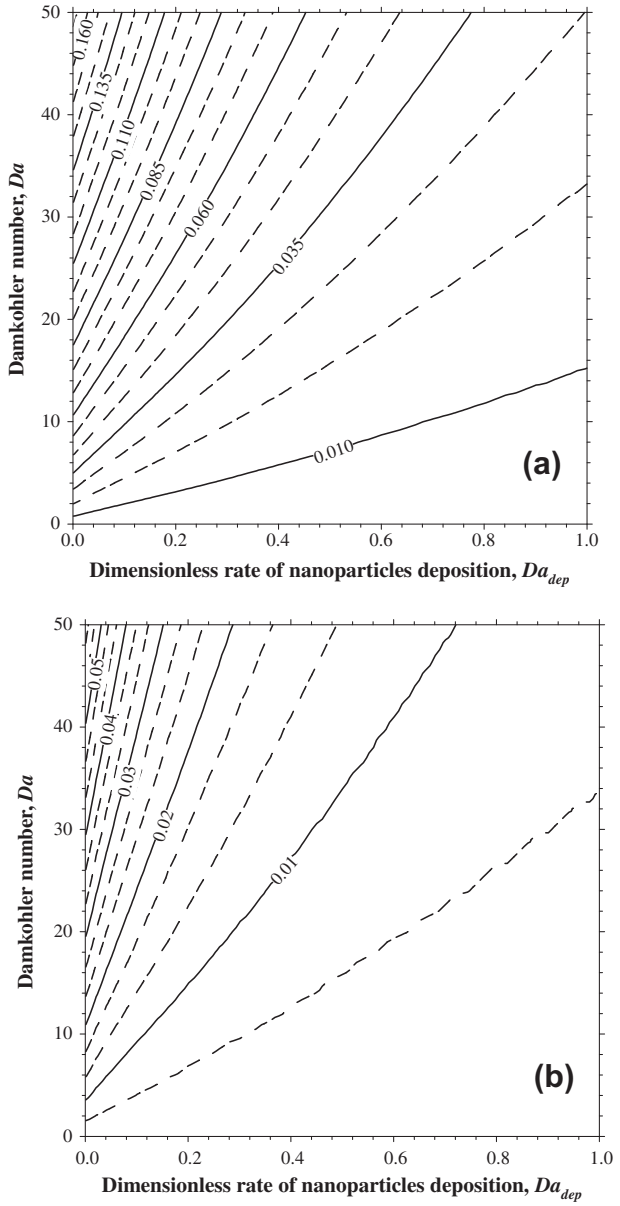

Fig. 16. Contours of maximum growth rates for different Damkohler numbers and deposition rates, $t_0 = 2$: (a) $c_{c0} = 0.01$; (b) $c_{c0} = 0.002$.

rates of deposition is more unstable at similar times. This may be considered as a general conclusion, if different Damköhler numbers and nano-catalyst concentrations do not change the trend. All cases reach extrema and descend to limiting small values. The examination reveals that the maximum growth rate keeps its decreasing trend at very long times, but with a very small slope. Basically, this trend describes the stabilizing and destabilizing effects of diffusion and shows that it is not affected by the rate of nanoparticle deposition.

Fig. 16 illustrates the contours of ω_{max} for different deposition rates and Damköhler numbers at two different concentrations of nano-catalysts. The contours shrink to smaller values as the concentration of nanoparticles decreases. The figure shows that the flow system at the highest Damköhler number and the smallest deposition rate is always more unstable. Indeed, the contours illustrate that any factor that results in an increment in the rate of reaction would make the flow system more unstable.

5. Summary and conclusions

Nano-catalytic reactions in porous media have recently been tested, both experimentally and theoretically, with application in environmental remediation and heavy oil upgrading. A detailed linear stability analysis has been conducted to show how the Brownian motion of the nanoparticles as nano-catalysts in homogeneous saturated porous media may affect the stability of a reactive front. Using the quasi-steady state approximation, the eigenvalue problem has been solved analytically and numerically to find the corresponding perturbation growth rate of each wavenumber.

It has been shown that the stability of the system is highly affected by the addition of nanoparticles as nano-catalysts. In particular, we have found that increasing the reaction rate increases the front instability by shifting the vortices upstream. The diffusion of both particles and liquids have been found to have an initial destabilizing effect, but can later have a destabilizing influence. The nanoparticle diffusion coefficient has been shown to stabilize the front when its values are very small or large enough; otherwise, the flow system is unstable. Increasing the nano-catalysts deposition rate has been also found to have a stabilizing effect. In general, factors that cause the reaction to be expedited were found to have a destabilizing impact on the front. The results have revealed that increasing nano-catalysts behind the front destabilizes the front as the reaction rate increases.

It is necessary to mention that all above analyses have been based on an isothermal system. However, the results may be changed if the reaction release or absorb heat. For instance, In this case of heat generation, if reduction in viscosity of displaced fluid as a result of temperature increase is larger than displacing fluid, then we might see a stabilizing effect due to heat generation at the interface. However, if reduction in viscosity of the displaced fluid by heat generation is less in displaced fluid, then the heat generation might have destabilizing effects.

At this stage, the present work should guide future experimental and numerical investigations of nano-fluidics in porous media by giving stability trends in the controlling parameters space. Further work in this direction is in progress.

Acknowledgments

The financial support of the Alberta Ingenuity Centre for *In Situ* Energy (AICISE) is acknowledged. The authors acknowledge helpful comments from G.M. Homsy, J. of University of British Columbia and J. Azaiez, H. Emami Meybodi, and S.H. Hejazi of University of Calgary.

References

[1] Pelley AJ, Tufenkji N. Effect of particle size and natural organic matter on the migration of nano- and microscale latex particles in saturated porous media. J Colloid Interface Sci 2008;321(1):74–83.
[2] Johari WLW, Diamessis PJ, Lion LW. Mass transfer model of nanoparticle-facilitated contaminant transport in saturated porous media. Water Res 2009;44(4):1028–37.
[3] Doshi R, Braida W, Christodoulatos C, Wazne M, O'Connor G. Nano-aluminum: transport through sand columns and environmental effects on plants and soil communities. Environ Res 2008;106(3):296–303.
[4] Kanel S, Nepal D, Manning B, Choi H. Transport of surface-modified iron nanoparticle in porous media and application to arsenic(III) remediation. J Nanopart Res 2007;9(5):725–35.
[5] Saleh N, Sirk K, Liu Y, et al. Surface modifications enhance nanoiron transport and napl targeting in saturated porous media *Environ.* Eng Sci 2007;24(1):45–57.
[6] Hydutsky BW, Mack EJ, Beckerman BB, Skluzacek JM, Mallouk TE. Optimization of nano- and microiron transport through sand columns using polyelectrolyte mixtures. Environ Sci Technol 2007;41(18):6418–24.

[7] Phenrat T, Saleh N, Sirk K, Tilton RD, Lowry GV. Aggregation and sedimentation of aqueous nanoscale zerovalent iron dispersions. Environ Sci Technol 2006;41(1):284–90.
[8] Liu X, Wazne M, Christodoulatos C, Jasinkiewicz KL. Aggregation and deposition behavior of boron nanoparticles in porous media. J Colloid Interface Sci 2009;330(1):90–6.
[9] Frey JM, Schmitz P, Dufreche J, Gohr Pinheiro I. Particle deposition in porous media: analysis of hydrodynamic and weak inertial effects. Transp Porous Media 1999;37(1):25–54.
[10] Przekop R, Gradon L. Deposition and filtration of nanoparticles in the composites of nano- and microsized fibers. Aerosol Sci Technol 2008;42(6):483–93.
[11] Kim J-Y, Cohen C, Shuler ML, Lion LW. Use of amphiphilic polymer particles for in situ extraction of sorbed phenanthrene from a contaminated aquifer material. Environ Sci Technol 2000;34(19):4133–9.
[12] Ghesmat K, Hassanzadeh H, Abedi J, Chen Z. Influence of nanoparticles on the dynamics of miscible Hele-Shaw flows. J Appl Phys 2011;109(10):104907–15.
[13] Iwasaki T. Some notes on sand filtration. J AWWA 1937;29:1591–957.
[14] Payatakes AC, Tien C, Turian RM. A new model for granular porous media: Part i. Model formulation. AIChE J 1973;19(1):58–67.
[15] Rajagopalan R, Kim JS. Adsorption of Brownian particles in the presence of potential barriers: effect of different modes of double-layer interaction. J Colloid Interface Sci 1981;83(2):428–48.
[16] Spielman LA, Friedlander SK. Role of the electrical double layer in particle deposition by convective diffusion. J Colloid Interface Sci 1974;46(1):22–31.
[17] Gruesbeck C, Collins RE. Entrainment and deposition of fine particles in porous media. SPE J 1982;22(6):847–56.
[18] Sharma MM, Yortsos YC. Transport of particulate suspensions in porous media: model formulation. AIChE J 1987;33(10):1636–43.
[19] Ghosh MM, Porter RL, Jordan TA. Physicochemical approach to water and wastewater filtration. J Environ Eng Div 1975;101(1):71–86.
[20] Adamczyk Z. Particle transfer and deposition from flowing colloid suspensions. Colloids Surf 1989;35(2):283–308.
[21] Elimelech M, O'Melia CR. Kinetics of deposition of colloidal particles in porous media. Environ Sci Technol 1990;24(10):1528–36.
[22] Hejazi SH, Trevelyan PMJ, Azaiez J, De Wit A. Viscous fingering of a miscible reactive $A + B \rightarrow C$ interface: a linear stability analysis. J Fluid Mech 2010;652:501–28.
[23] De Wit A, Homsy GM. Viscous fingering in reaction–diffusion systems. J Chem Phys 1999;110(17):8663–75.
[24] Nagatsu Y, Kondo Y, Kato Y, Tada Y. Effects of moderate Damköhler number on miscible viscous fingering involving viscosity decrease due to a chemical reaction. J Fluid Mech 2009;625:97–124.
[25] Fernandez J, Homsy GM. Viscous fingering with chemical reaction: effect of in-situ production of surfactants. J Fluid Mech 2003;480:267–81.
[26] Hill S. Channeling in packed columns. Chem Eng Sci 1952;1(6):247–53.
[27] Saffman PG, Taylor G. The penetration of a fluid into a porous medium or Hele-Shaw cell containing a more viscous liquid. Proc R Soc Lond A 1958;245(1242):312–29.
[28] Park CW, Homsy GM. The instability of long fingers in Hele-Shaw flows. Phys Fluids 1985;28(6):1583–5.
[29] Nittmann J, Daccord G, Stanley HE. Fractal growth viscous fingers: quantitative characterization of a fluid instability phenomenon. Nature 1985;314(6007):141–4.
[30] Brener E, Levine H, Tu Y. Nonsymmetric Saffman-Taylor fingers. Phys Fluids A 1991;3(4):529–34.
[31] Mishra M, Martin M, De Wit A. Miscible viscous fingering with linear adsorption on the porous matrix. Phys Fluids 2007;19(7):073101–9.
[32] Zhao H, Maher JV. Associating-polymer effects in a Hele-Shaw experiment. Phys Rev E 1993;47(6):4278–83.
[33] Peaceman DW, Rachford Jr HH. Numerical calculation of multidimensional miscible displacement. SPE J 1962;2(4):327–39.
[34] Yortsos YC, Zeybek M. Dispersion driven instability in miscible displacement in porous media. Phys Fluids 1988;31(12):3511–8.
[35] Ghesmat K, Azaiez J. Viscous fingering instability in porous media: effect of anisotropic velocity-dependent dispersion tensor. Transp Porous Media 2008;73(3):297–318.
[36] Tan CT, Homsy GM. Stability of miscible displacements in porous media: rectilinear flow. Phys Fluids 1986;29(11):3549–56.
[37] Manickam O, Homsy GM. Stability of miscible displacements in porous media with nonmonotonic viscosity profiles. Phys Fluids A 1993;5(6):1356–67.
[38] Ruith M, Meiburg E. Miscible rectilinear displacements with gravity override. Part I. Homogeneous porous medium. J Fluid Mech 2000;420:225–57.
[39] Hoffman BD, Shaqfeh ESG. The effect of Brownian motion on the stability of sedimenting suspensions of polarizable rods in an electric field. J Fluid Mech 2009;624:361–88.
[40] Ennis-King J, Preston I, Paterson L. Onset of convection in anisotropic porous media subject to a rapid change in boundary conditions. Phys Fluids 2005;17(8):084107–21.
[41] Riaz A, Hesse M, Tchelepi HA, Orr FM. Onset of convection in a gravitationally unstable diffusive boundary layer in porous media. J Fluid Mech 2006;548:87–111.
[42] Hassanzadeh H, Pooladi-Darvish M, Keith DW. Stability of a fluid in a horizontal saturated porous layer: effect of non-linear concentration profile, initial, and boundary conditions. Transp Porous Media 2006;65(2):193–211.
[43] Hassanzadeh H, Pooladi-Darvish M, Keith DW. Modeling of convective mixing in CO_2 storage. J Can Pet Technol 2005;44(10):43–51.
[44] Armento ME, Miller CA. Stability of moving combustion fronts in porous media. Soc Petrol Eng J 1977;17(6):423–30.
[45] Britten JA, Krantz WB. Linear stability of planar reverse combustion in porous media. Combust Flame 1985;60(2):125–40.
[46] Levenspiel O. Chemical reaction engineering. Wiley; 1999.
[47] Tien C. Granular filtration of aerosols and hydrosols. Boston: Butterworths; 1989.
[48] Ruckenstein E, Prieve DC. Adsorption and desorption of particles and their chromatographic separation. AIChE J 1976;22(2):276–83.
[49] Chu Y, Jin Y, Yates MV. Virus transport through saturated sand columns as affected by different buffer solutions. J Environ Qual 2000;29(4):1103–10.
[50] Jin Y, Yates MV, Thompson SS, Jury WA. Sorption of viruses during flow through saturated sand columns. Environ Sci Technol 1997;31(2):548–55.
[51] Civan F. Evaluation and comparison of the formation damage models. In: SPE formation damage control symposium. Lafayette, Louisiana, USA: Society of Petroleum Engineers; 1992. p. 219–36.
[52] Civan F. A multi-phase mud filtrate invasion and well bore filter cake formation model. In: International petroleum conference and exhibition of Mexico. Veracruz, Mexico: Society of Petroleum Engineers; 1994. p. 399–412.
[53] Kreyszig E. Advanced engineering mathematics. 9th ed. John Wiley & Sons; 2006.
[54] Mackay ME, Dao TT, Tuteja A, et al. Nanoscale effects leading to non-Einstein-like decrease in viscosity. Nat Mater 2003;2(11):762–6.
[55] Rudyak VY, Dubtsov SN, Baklanov AM. Temperature dependence of the diffusion coefficient of nanoparticles. Tech Phys Lett 2008;34(6):519–21.
[56] d'Orlyé F, Varenne A, Gareil P. Determination of nanoparticle diffusion coefficients by Taylor dispersion analysis using a capillary electrophoresis instrument. J Chromatogr A 2008;1204(2):226–32.
[57] Einstein A. Eine neue bestimmung der moleküldimensionen. Ann Phys 1906;324(2):289–306.